

Electronic Supplementary Information

High-yield production of 2D crystals by wet-jet milling

A. E. Del Rio Castillo^{a*}, V. Pellegrini^{a,b}, A. Ansaldo^a, F. Ricciardella^a, H. Sun^a, L. Marasco^a, J. Buha^c, Z. Dang^c, L. Gagliani^a, E. Lago^a, N. Curreli^a, S. Gentiluomo^a, F. Palazon^c, M. Prato^c, R. Oropesa-Nuñez^b, P. Toth^a, E. Mantero^a, M. Crugliano^a, A. Gamucci^a, A. Tomadin^a, M. Polini^a, and F. Bonaccorso^{a,b*}

^a Istituto Italiano di Tecnologia. Graphene Labs. Via Morego 30. 16163, Genoa, Italy.

^b BeDimensional Srl. Via Albisola 121. 16163, Genova, Italy.

^c Istituto Italiano di Tecnologia. Nanochemistry Department. Via Morego 30. 16163, Genoa, Italy.

* Corresponding authors: antonio.delrio@iit.it; francesco.bonaccorso@iit.it.

Raman peaks assignment of graphene-graphite flakes

The Raman spectrum of graphene is composed by several characteristic peaks. The G peak, positioned at $\sim 1585\text{ cm}^{-1}$, which corresponds to the E_{2g} phonon at the Brillouin zone centre.^{1,2} The D peak, which is due to the breathing modes of the sp^2 hybridized carbon rings requiring a breaking on the carbon-ring symmetry for its activation by double resonance. Double resonance also happens as an intra-valley process, i.e., connecting two points belonging to the same cone around K or K',² resulting in the rise of the D' peak. The 2D peak (a second order resonance of the D band) centred at $\sim 2680\text{ cm}^{-1}$ for an excitation wavelength of 514.5nm in case of a single layer graphene.² For few and multi-layer graphene the 2D peak is a superposition of multiple components, the main being the 2D₁ and 2D₂ components.³ The 2D peak is always present, since no defects are required for the activation of two phonons with the same momentum, one being backscatter from the other.² In graphite, the intensity of the 2D₂ band is roughly twice the 2D₁ band,² while for mechanically exfoliated single layer graphene (SLG) the 2D band is a single and sharp peak, which is roughly 4 times more intense than the G peak.³

Evaluation of lateral size and thickness of the exfoliated flakes

As discussed in Ref. 4 the exfoliation of 2D crystals is considered as a fragmentation process. This means that the size distribution of the flakes follows a log-normal distribution. Following this model, all the lateral size and thickness values reported in the main text corresponds to the distribution mode, which is the most frequent value in a data set (i.e., the distribution peak).

The lateral sizes and thicknesses standard deviation are log-normal standard deviations. **Figure S1** shows the difference between the mode and the mean for a log-normal distribution.

Surface tension-surface energy relationship

In order to exfoliate and stabilize a 2D crystal in a solvent, as stated in the main text, the Gibbs free energy of the mixture solvent/layered material should be minimized.^{5,6,7,8} This condition can be fulfilled if the solvent

surface tension is equivalent to the surface energy of the material by using the equation⁵

$$\gamma = E_{Surface}^{Solvent} - TS_{Surface}^{Solvent} \quad \text{Eq.S1}$$

in which, E is the solvent surface energy, T is the absolute temperature and S is the solvent surface entropy, having a value of $10^{-3}\text{ J m}^{-2}\text{ K}^{-1,5,9,10}$

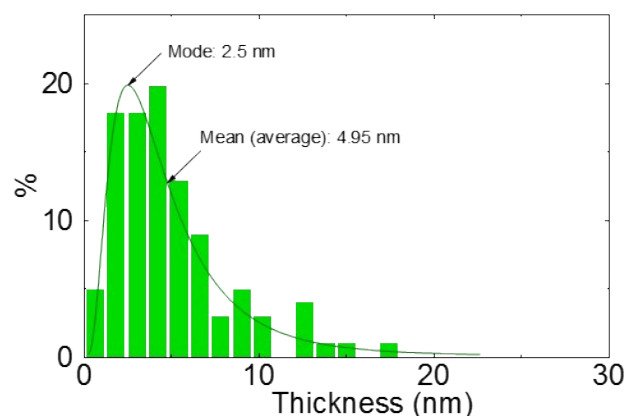


Figure S1. Log-normal distribution of exfoliated WS₂ flakes.

Characterization of the exfoliated samples

Additional high resolution transmission electron microscopy (HRTEM) images of the sample WJM0.10 are presented in **Figure S2**. The images show the edge zone of bended flakes. The image contrast in the bended edge is larger than in the flake basal plane, making it possible to directly count the number of layers. The number of layers is highlighted in white; the insets are the fast Fourier transformation of selected zones on each image, showing the characteristic honeycomb lattice of graphene.

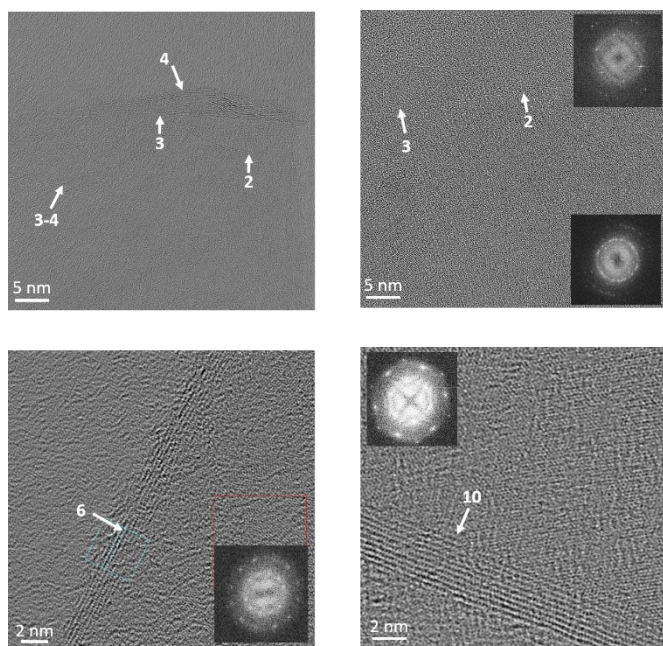


Figure S2. HRTEM images at the edge of bended flakes from the sample WJM0.10.

In order to evaluate the presence of functional groups on the exfoliated flakes, due to possible reaction with the solvent, we performed Fourier Transform Infrared spectroscopy (FTIR). The processed WJM0.30, WJM0.5 and WJM0.10 samples as well as the bulk graphite are washed to avoid contribution from solvent residuals, see the Experimental part in the main text for details. The FTIR of all the samples do not revealed the presence of functional groups or solvents (**Figure S3**). Literature indicates that expected functional groups peaks are at 1080 to 1360 cm^{-1} for C-N, stretching vibration bonding, from 3300-2500 cm^{-1} , 1440-1395 and 950-910 cm^{-1} for O-H, from 1760-1690 cm^{-1} for C=O, and from 1320-1210 cm^{-1} for C-O bonding.¹¹ The FTIR characterization of our samples reveals no presence of those groups. However, the exfoliation and fragmentation of bulk graphite is expected to produce oxygen groups at the flake edges.^{12,13,14} The absence of peaks in the FTIR spectra suggest that these functional groups are below the instrument sensitivity. Thus, in order to have a proof of the presence and nature of functional groups in the exfoliated flakes, we performed high resolution X-ray photoelectron spectroscopy (XPS). **Figure S3 b, c** and **d** report the carbon, oxygen and nitrogen peaks, respectively. By calculating the areas under the carbon, oxygen and nitrogen peaks, and after the normalization to the corresponding relative sensitivity factors (*i.e.*, factors related to the cross-section of the photoemission process),¹⁵ we evaluated the surface composition of the three samples. The results of the quantitative analysis are reported in the **Table S1**. The lack of correlation between the samples regarding the presence of nitrogen and oxygen groups lead us to conclude that the presence of these atoms are mainly related to traces of

	C (at.%)	O (at.%)	N (at.%)	O/C
WJM0.30	91.4	7.4	1.2	0.08
WJM0.15	92.7	6.8	0.5	0.07
WJM0.10	93.5	6.0	0.5	0.06
WJM0.10 centrifuged	95.2	4.2	0.5	0.04

groups.

solvent rather than functional groups.

Table S1. XPS quantitative analysis

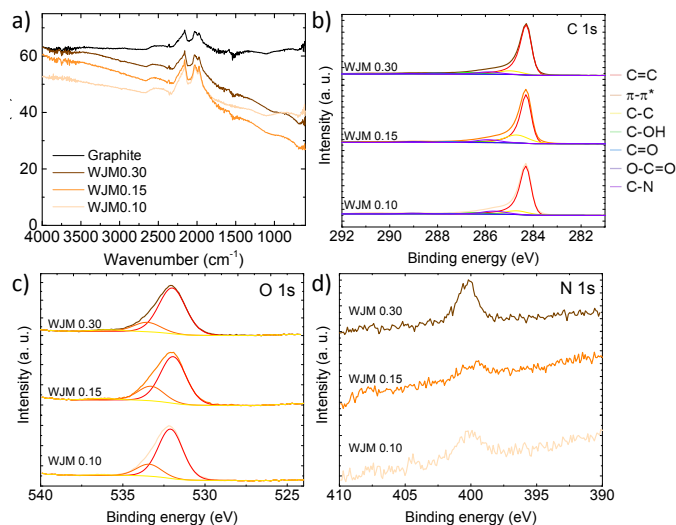


Figure S3. a) Fourier transform infra-red spectra. X-ray photoemission spectroscopy of the processed samples resolved for b) C 1s, c) O 1s and d) N 1s.

Exfoliation of graphite in surfactants-aided aqueous solution

For the exfoliation of graphite in water and sodium cholate we followed the same protocol used for the exfoliation in organic solvents, *i.e.*, consecutively using the 0.30, 0.15 and twice the 0.10 mm nozzle. **Figure S4a** shows a representative image of few-layers graphene on a TEM grid, the inset (top left) shows the electron diffraction pattern, demonstrating the crystalline structure of the flake. The lateral size statistical distribution peaks at 220 nm, **Figure S4b**, with a lognormal standard deviation of 0.89. The thickness of the exfoliated flakes is estimated by atomic force microscopy (AFM).

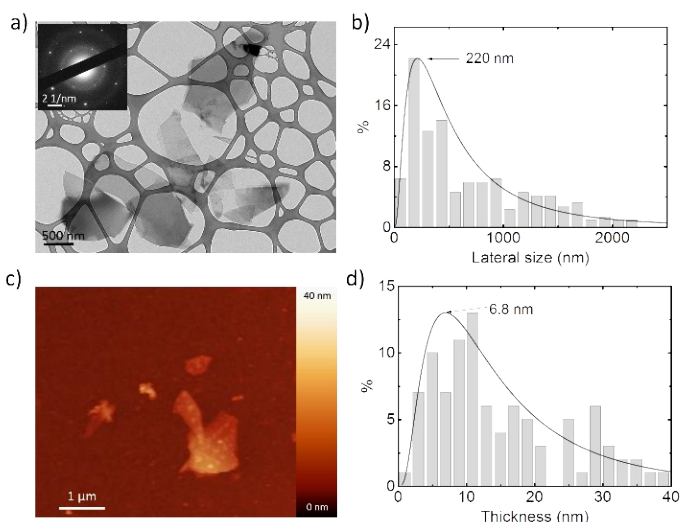


Figure S4c shows a characteristic flake, while the statistical thickness distribution peaks at 6.8 nm with a lognormal standard deviation of 0.78.

Figure S4. a) Representative TEM image of exfoliated flakes in water and sodium cholate. b) Statistical lateral size distribution analysing 200 flakes. c)

Representative AFM image of exfoliated flakes and d) their thickness distribution.

Spectroscopy analysis of centrifuged WJM0.10

The statistics of the Raman spectra acquired on samples prepared at different centrifugation speeds is analysed in order to understand the relative change between graphene/few-layer graphene and multi-layer graphene flakes during the purification process. The $I(D)/I(G)$ statistical distribution broads when the centrifugal speed increases (Figure S5 a), ranging from 0.03 to 1.2, for WJM0.10 samples, increasing to 2 for the WJM0.10-3000g.

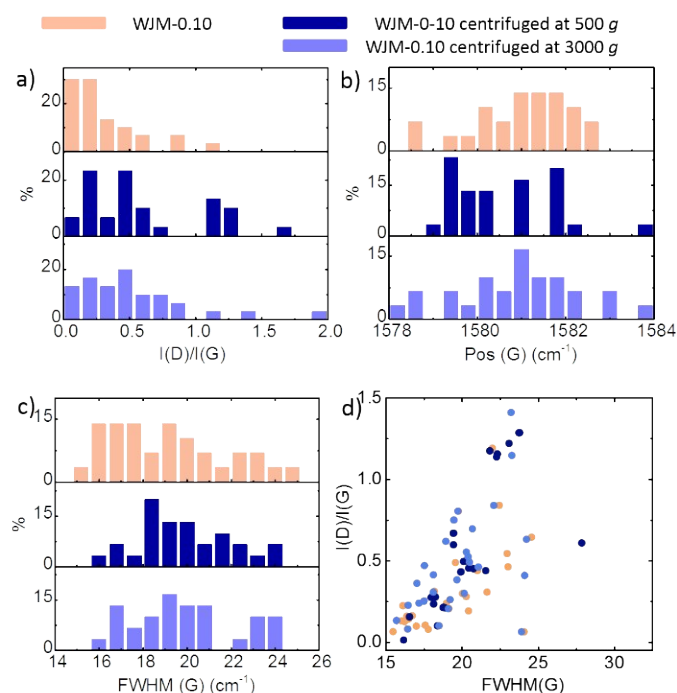


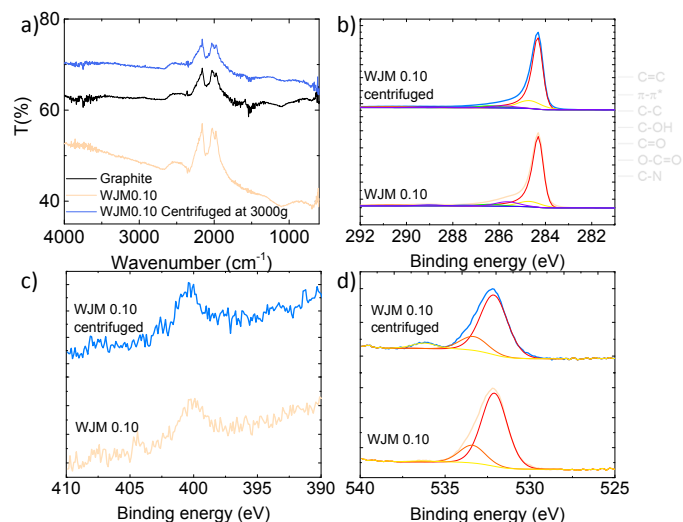
Figure S5. Statistical Raman analysis of the purified samples (dark and light blue or centrifuged at 500 and 3000 g, respectively) compared with the as-produced WJM0.10 sample. a) $I(D)/I(G)$, b) Pos(G), c) FWHM(G) and d) Pos(2D).

The G peak position (Pos(G)) and its full width at half maximum (FWHM (G)) of the Raman spectra of the purified samples after ultracentrifugation are unchanged compared with the ones of the as-prepared sample. This indicates that no changes in doping and creation of defects are promoted by the ultracentrifugation process (Figure S5 b-d). To understand the nature of the defects, specifically, the type of functional groups on the flake edges, FTIR and XPS are performed on the centrifuged sample at 3000 g. The FTIR spectra, as in the case of the as-produced samples, do not show either the presence of solvent traces or functional groups, Figure S6 a. The high resolution XPS reveals the presence of oxygenated and nitrogen groups in the centrifuged sample, Figure S6 b to d. The presence of nitrogen, from solvent residual is analysed by the N spectra of XPS. Table S1 specifies the atomic percentage on the samples surface.

Figure S6. Analysis of functional groups in the purified WJM0.10 sample by (a) FTIR and X-ray photoemission spectroscopy resolved for (b) C 1s, (c) O 1s and (d) N 1s

Exfoliation and characterization of other layered materials

Optical absorption spectroscopy of MoS_2 , WS_2 and $h\text{-BN}$



The spectrum of MoS_2 is characterized by two excitonic bands, originating from the inter-band excitonic transition at the K point of the Brillouin zone and are located at 671 nm and 613 nm.^{16,17,18} In the case of WS_2 , the spectrum shows two main peaks around 530 nm and 639 nm corresponding to the excitonic absorption bands arising from the gap transition at the K point of the Brillouin zone.¹⁹ The $h\text{-BN}$ spectrum shows no bands in the wavelength range between 400 nm and 800 nm, but it is usually characterized by a band located at 236 nm corresponding to an optical band gap of ~ 5.26 eV, as it is shown in the reported literature on exfoliated $h\text{-BN}$ nanosheets.^{8,20} However, in this range there is the cut-off absorption of NMP (285 nm), thus making impossible to observe the aforementioned peak.

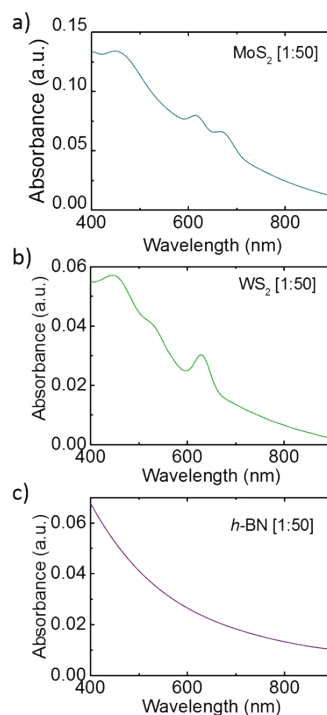


Figure S7. Optical absorption spectra of a) MoS₂, b) WS₂ and c) h-BN.

The concentration of the dispersions obtained through UV-visible spectroscopy is reported in Table S2. All the extinction coefficients (α) and the reference wavelength (λ) used to calculate the concentrations are taken from the value reported in Ref 5. The optical extinction coefficient is determined by using the Beer-Lambert law ($E = \alpha Cl$, in which E is the optical extinction at 600 nm, C the concentration of the exfoliated 2D crystal and l is the path length, 0.01 m)

Table S2. Concentration and extinction coefficients

Material	α [Lm/g]	λ [nm]	C [g/L]
MoS ₂	3400	672	0.05
WS ₂	2756	629	0.7
h-BN	2367	300	0.15

Raman spectroscopy and statistics of MoS₂, WS₂ and h-BN

The Raman spectra of bulk MoS₂ exhibits two main peaks, the first one, *i.e.*, the A_{1g}, located at 405 cm⁻¹ and E_{2g} positioned at 379 cm⁻¹.¹⁷ The A_{1g} is due to the in-plane vibration of the molybdenum and sulphur atoms, and the E_{2g} corresponds to the out-of-plane vibration.²¹ The shifting of the two peaks with respect to the bulk ones indicates a reduction of the number of layers compared to the bulk counterpart. This behaviour has been discussed previously in literature.^{8,22,23,24} Moreover, the peaks in the exfoliated material show a broadening with respect to the bulk peaks, which also indicates a decrease in the flakes thickness, as observed in the study of Ramakrishna Matte et al.²⁵

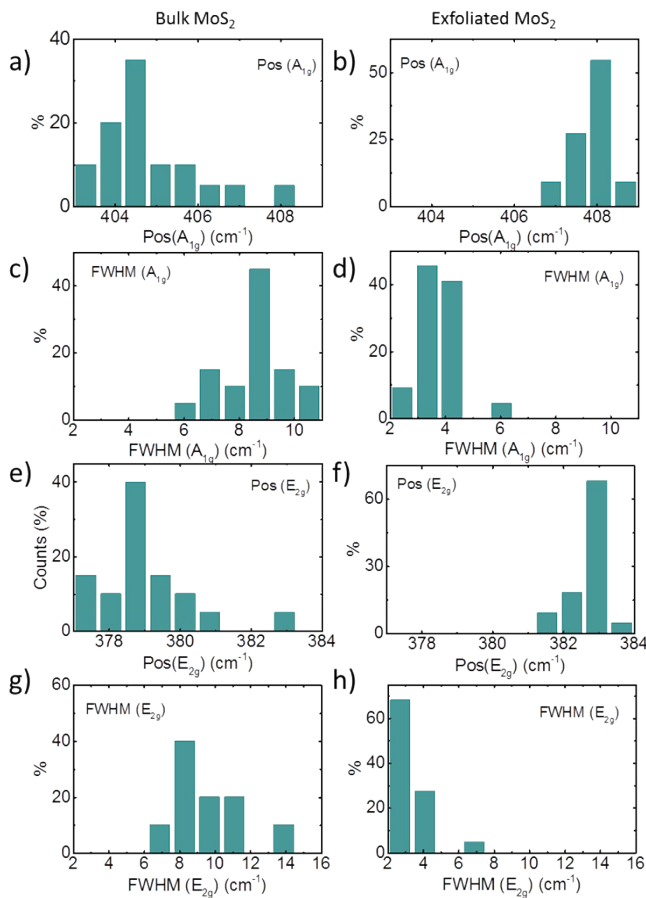


Figure S8 Raman statistical analysis of bulk and exfoliated MoS₂.

The comparison between the Raman spectra of the as-produced WS₂ flakes and the bulk WS₂ powder are reported in **Figure S9**. The Raman spectrum of WS₂ consists mainly in three peaks, the first-order modes at the Brillouin zone centre E_{12g}(Γ) and A_{1g}(Γ), which involve the in-plane displacement of W and S atoms and the out-of-plane displacement of S atoms, respectively.^{26,27,28,29} The second order longitudinal acoustic mode at the M point, 2LA(M).^{26-30,31,32,33,34} The E_{12g}(Γ) of single-/few-layer flakes of WS₂, located at ~421 cm⁻¹, is stiffened with respect to the bulk WS₂, which is generally found at ~419 cm⁻¹.²⁶⁻³⁰ The blue-shift of the E_{12g}(Γ) Raman mode in WS₂ flakes results from the reduced dielectric screening of long range Coulomb interaction with respect to the bulk WS₂.²⁶⁻³⁴ The 2LA(M) overlaps the E_{12g}(Γ), despite of this the multi-peak Lorentzian fitting separates their

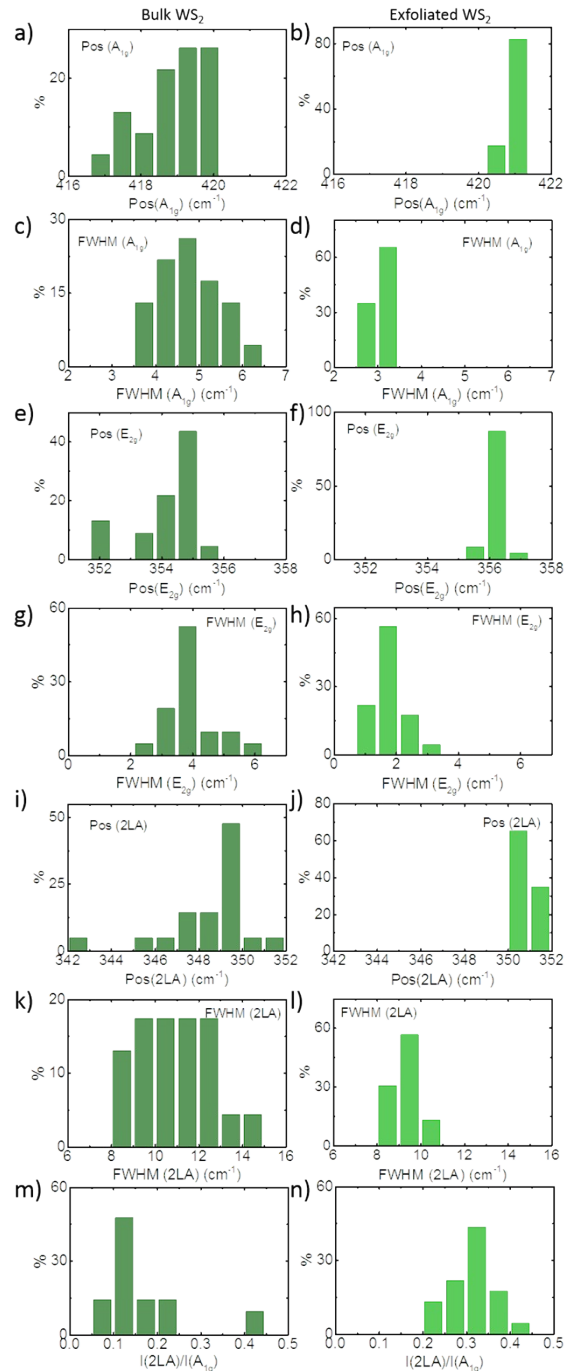


Figure S9 Raman statistical analysis of bulk and exfoliated WS₂.

individual contributions, as shown in **Figure 5h**. The analysis of the ratio of the intensity of the peak $2LA(M)$ and $A_{1g}(\Gamma)$, has been used to assess the single-/few-layer composition of WS_2 samples.²⁸ In our case, the spectra analysis estimates $I(2LA)/I(A_{1g})$ values ~ 0.2 in bulk WS_2 and ~ 0.35 in the exfoliated few-layer WS_2 flakes.

The bulk hexagonal boron nitride exhibits a characteristic peak positioned at 1366 cm^{-1} that is due to in-plane atomic displacements,^{35,36,29} The exfoliation of the h -BN from the bulk material to few layer or bilayer flakes is associated to a red shift of the peak E_{2g} .^{37,38,39}

Statistical analysis (performed on 106 flakes) of the E_{2g} peak position shows the maximum distribution of the $\text{Pos}(E_{2g})$ down shifted of 1 cm^{-1} , *i.e.*, from 1366.6 cm^{-1} bulk to 1365.5 cm^{-1} , from the exfoliated samples, respectively, demonstrating the thinning of the h -BN flakes.^{29,30,31}

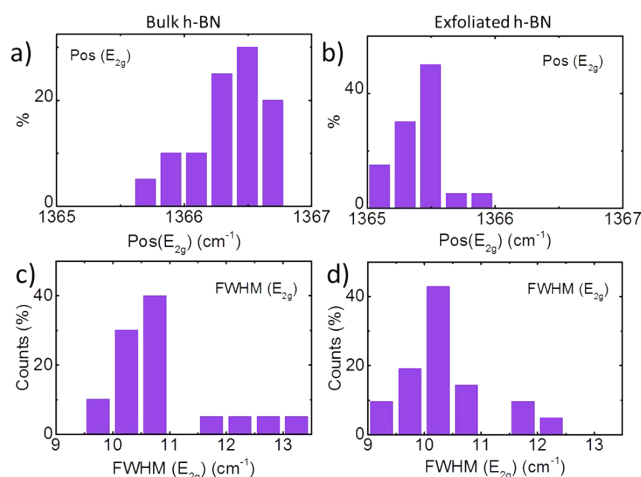


Figure S10 Raman statistical analysis of bulk and exfoliated h -BN.

References

- 1 L. Yang, J. Deslippe, C.-H. Park, M. L. Cohen and S. G. Louie, *Phys. Rev. Lett.*, 2009, **103**, 186802.
- 2 A. C. Ferrari and D. M. Basko, *Nature Nanotech.*, 2013, **8**, 235.
- 3 A. C. Ferrari, J. C. Meyer, V. Scardaci, C. Casiraghi, M. Lazzeri, F. Mauri, S. Piscanec, D. Jiang, K. S. Novoselov, S. Roth and A. K. Geim, *Phys. Rev. Lett.*, 2006, **97**, 187401.
- 4 K. Kouroupis-Agalou, A. Liscio, E. Treossi, L. Ortolani, V. Morandi, N. M. Pugno, and V. Palermo, *Nanoscale*, 2014, **6**, 5926.
- 5 Y. Hernandez, V. Nicolosi, M. Lotya, F. M. Blighe, Z. Sun, S. De, I. T. McGovern, B. n. Holland, M. Byrne, et al., *Nat. Nanotechnol.*, 2008, **3**, 563.
- 6 Coleman, J. N. *Adv. Funct. Mater.* 2009, **19**, 3680–3695.
- 7 Hansen, C. *Hansen Solubility Parameters: A user's handbook*, Second Edition. Boca Raton, Fla: CRC Press. 2007, ISBN 978-0-8493-7248-3.
- 8 Coleman, J. N.; Lotya, M.; O'Neill, A.; Bergini, S. D.; King, P. J.; Kan, U.; Young, K.; Gaucher, A.; De, S.; Smith, R. J.; et al. *Science*. 2011, **331**, 568-571.
- 9 Lyklema, J. *Colloids Surf. A*. 1999, **156**, 413.
- 10 A. E. Del Rio-Castillo, C. Merino, E. Díez-Barra and E. Vázquez, *Nano Res.*, 2014, **7**, 963.
- 11 B. C. Smith. *Fundamentals of Fourier Transform Infrared Spectroscopy*, Second Edition. CRS press 2011.
- 12 C. E. Halbig, T. J. Nacken, J. Walter, C. Damm, S. Eigler, W. Peukert, *Carbon*, 2016, **96**, 897.
- 13 J. Benson, Q. Xu, P. Wang, Y. Shen, L. Sun, T. Wang, M. Li, P. Papakonstantinou, *ACS Appl. Mater. Interfaces*, 2014, **6**, 19726.
- 14 U. Khan, A. O'Neill, M. Lotya, S. De, J. N. Coleman, *Small* 2010, **6**, 864.
- 15 E. Desimoni, B. Brunetti, *Chemosensors*, 2015, **3**, 70.
- 16 K. Wang, Y. Feng, C. Chang, J. Zhan, C. Wang, Q. Zhao, J. N. Coleman, L. Zhang, W. J. Blau, J. Wang, *Nanoscale*, 2014, **6**, 10530.
- 17 K. F. Mak, C. Lee, J. Hone, J. Shan, T. F. Heinz, *Phys. Rev. Lett.* 2010, **105**, 136805.
- 18 A. Splendiani, L. Sun, Y. Zhang, T. Li, J. Kim, C.-Y. Chim, G. Galli, F. Wang, *Nano Lett.* 2010, **10**, 1271.
- 19 A.K. Mishra, K. V. Lakshmi, L. Huang., *Scientific Reports*, 2015, **5**, 15718.
- 20 P. Thangasamy and M. Sathish, *Cryst. Eng. Comm.*, 2015, **17**, 5895.
- 21 C. Lee, H. Yan, L. E. Brus, T. F. Heinz, J. Hone, S. Ryu., *ACS Nano*, 2010, **5**, 2695.
- 22 B. Mao, Y. Yongbo, S. Yuchuan, Y. Bin, X. Zhengguo, H. Jinsong. *Nanosci. Nanotechnol. Lett.* 2014, **6**, 685.
- 23 H. Li Q. Zhang, C. C. Ray Yap, B. K. Tay, T. H. Tong E., A. Olivier, D. Baillarg, *Adv. Func. Mater.* 2012, **22**, 1385.
- 24 K. Wang, J. Wang, J. Fan, M. Lotya, A. O'Neill, D. Fox, Y. Feng, X. Zhang, B. Jiang, Q. Zhao., *ACS Nano*, 2013, **7**, 9260.
- 25 H. S. S. R. Matte, A. Gomathi, A. K. Manna, D. J. Late, R. Datta, S. K. Pati, C. N. R. Rao, *Angew. Chem. Int. Ed.* 2010, **49**, 4059.
- 26 A. Molina-Sanchez, L. Wirtz. *Phys. Rev. B*, 2011, **84**, 155413.

- 27 R. Saito, Y. Tatsumi, S. Huang, X. Ling, M. S. Dresselhaus, *J. Phys. Cond. Matter*, **2016**, *28*, 353002
- 28 A. Berkdemir, H. R. Gutiérrez, A. R. Botello-Méndez, N. Perea-López, A. L. Elías, C. I. Chia, B. Wang, V. H. Crespi, F. López-Urías, J. C. Charlier, H. Terrones, *Sci. Rep.* **2013**, *3*, 1755
- 29 M. Thripuranthaka, R. V. Kashid, C. Sekhar Rout, D. J. Late, *Appl. Phys. Lett.* **2014**, *104*, 081911;
- 30 C. Sourisseau, F. Cruege, M. Fouassier, M. Alba, *Chem. Phys.* **1991**, *150*, 281.
- 31 N. Peimyoo, J. Shang, W. Yang, Y. Wang, C. Cong, T. Yu, *Nano Res.* **2015**, *8*, 1210
- 32 Y. Chen, J. Xi, D. O. Dumcenco, Z. Liu, K. Suenaga, D. Wang, Z. Shuai, Y. S. Huang, L. Xie, *ACS Nano*, **2013**, *7*, 461
- 33 A. P. Gaur, S. Sahoo, J. F. Scott, R. S. Katiyar, *J. Phys. Chem. C*, **2015**, *119*, 5146
- 34 W. Zhao, Z. Ghorannevis, K. K. Amara, J. R. Pang, M. Toh, X. Zhang, C. Kloc, P. H. Tan, G. Eda, *Nanoscale*, **2013**, *5*, 9677.
- 35 R. Geick, C. Perry. *Phys. Rev. Lett.* 1966, **146**, 543.
- 36 A. Pakdel, Y. Bando and D. Golberg, *Chem. Soc. Rev.*, 2014, **43**, 934.
- 37 R. V. Gorbachev, I. Riaz, R. R. Nair, R. Jalil, L. Britnell, B. D. Belle, E. W. Hill, K. S. Novoselov, K. Watanabe, T. Taniguchi, *Small*, 2011, **7**, 4, 465.
- 38 J. Shang, F. Xue, C. Fan, E. Ding, *Materials Letters*, 2016, **181**, 144.
- 39 P. Thangasamy, M. Sathish, *Cryst. Eng. Comm*, 2015, **17**, 5895.